Quad-band circularly polarized super-wideband MIMO antenna for wireless applications

Quad-band circularly polarized super-wideband MIMO antenna for wireless applications

Amit Kumar[1] | Gaurav Saxena[2] | Preetam Kumar[3] | Yogendra Kumar Awasthi[4] | Priyanka Jain[5] | Sumer Singh Singhwal[6,7] | Prashant Ranjan[8]

[1]Department of Electronics & Communication Engineering, Bharati Vidyapeeth (Deemed to be University) College of Engineering, Pune, India

[2]Department of Electronics & Communication Engineering, Galgotia College of Engineering and Technology, Greater Noida, UP, India

[3]Department of Electrical Engineering, Indian Institute of Technology Patna, Bihta, Patna, India

[4]Antenna Fabrication & Measurement Laboratory, Electronics & Communication Engineering, Manav Rachna International Institute of Research and Studies, Faridabad, HR, India

[5]Department of Electronics & Communication Engineering, Delhi Technological University, Delhi, India

[6]Department of Electronics and Telecommunications, Politecnico di Torino, Torino, Italy

[7]Department of Electronics and Communication Engineering, Chandigarh University, Gharuan, Mohali, Punjab, India

[8]Department of Electronics & Communication Engineering, University of Engineering and Management, Jaipur, India

Correspondence
Gaurav Saxena, Department of Electronics & Communication Engineering, Galgotia College of Engineering and Technology, Greater Noida, UP 201306, India.
Email: gaurav.saxena@galgotiacollege.edu

Funding information
Ministry of Human Resource Development; National Project Implementation Unit (NPIU)

Abstract

In this article, a Super-wideband (2.6–22 GHz) two-elements multiple-input-multiple-output antenna (MIMO) is presented with a dimension of 49 54.5 1.6 mm^3 on an FR-4 substrate. The antenna is also exhibited dual circular polarization (RHCP and LHCP) simultaneously at two separate ports at four frequencies of 5.2, 11.5, 14.66, and 16.75 GHz, which are extensively utilized for WLAN, X, and Ku-band applications. Four EBG cells of various sizes have been installed across the feed line to maintain the antenna's efficiency and control the specific absorption rate (SAR). The antenna has a minimum isolation of 17 dB (20 dB for the important portion) in Super-wideband (SWB) and excellent diversity performance. Simulated results of antenna-like return loss, isolation, and diversity parameters have also been verified experimentally, which are in the acceptable range. Also, the calculated maximum SAR at 10 g is 1.095 W/kg with the head voxel model at 3.5 GHz.

KEYWORDS

left hand circularly polarized, multiple-input-multiple-output, right hand circularly polarized, super-wideband

1 | INTRODUCTION

Wireless communication has demanded better channel capacity with a high data rate in the current era. To fulfill this demand, the multiple-input-multiple-output (MIMO)-communication system that uses different antennas on the transmitter and receiver ends is developed. From the base station, multiple antennas transmit a signal to the mobile handset as shown in Figure 1, which acts as a receiver, provides better signal strength and a high data rate in

comparison to a single antenna element or single-input-single-output (SISO) system. MIMO antenna will increase the data throughput without requiring additional spectrum and repeaters. Better spatial diversity in the MIMO system will ensure a low correlation among antenna elements and will ensure less signal dropout in a multipath and fading environment. Several MIMO antennas have been designed in the literature to improve their characteristics in terms of impedance bandwidth, miniaturization, & isolation improvement.[1,2]

Keeping the aim of compactness in mind several MIMO antennas have been demonstrated with high isolation among antenna elements in the existing literature till now.[1,2] A compact planar multi-band antenna has been designed based on a Right Hand/Left-Hand transmission line for mobile applications.[3] A substrate integrated magneto-electric (ME) dipole antenna with metasurface has been proposed for 5G/WiMAX/WLAN/X-Band MIMO applications with a high gain of almost 9 dBi and low profile.[4] Meander line-inspired four-port compact MIMO antenna has been considered in Reference 5 for WLAN application. Modified Sierpinski carpet fractal geometry[6] has been introduced in the antenna design to maximize surface area utilization. Fractal geometry like Minkowski geometry[7–9] has been also useful in enhancing isolation among antenna elements in a MIMO system. A hepta-band Swastik arm MIMO antenna based on hybrid Quadric–Koch island fractal geometry for size miniaturization has been presented for mobile phone applications.[10] A miniaturized hook-shaped multi-band MIMO antenna has been presented in Reference 11 for mobile applications. A high isolation-based dual-polarized wideband MIMO antenna was depicted in Reference 12 for multiple wireless applications. Another high isolation two-element MIMO slot antenna for Eight-Band LTE/WWAN operation has been discussed in Reference 13. While in one case dual-layer electromagnetic band gap (EBG) has been used to design a miniaturized multi-element antenna for a MIMO system operating at 2.5 GHz with minimum isolation of 28 dB.[14] A complementary-split-ring-resonator (CSRR) loaded compact multi-band MIMO antenna has achieved high isolation due to the split-ring-resonator (SRR) placed between face-to-face antenna elements.[15] To maximize the isolation between elements of an antenna array, a transmission line-based decoupling structure was discussed in Reference 16. A compact dual-band slot antenna with high isolation of 21 dB has been achieved by using Defected Ground Structure (DGS) by creating a wide slot in the ground plane for WLAN application.[17] In Reference 18, a tri-polarized MIMO antenna having an omnidirectional radiation pattern and low correlation has been presented. Without a common ground plane, the MIMO antenna results in much higher isolation without any decoupling techniques.[19] In Reference 20, perpendicularly arranged 10 elements of antenna array have been introduced for sub-6 GHz 5G mobile application, which provides better channel capacity, high data rate, and high isolation.

The circularly polarized antenna has been extensively designed due to its wide applicability in state-of-art technology as CP antennas can inhibit the losses due to polarization mismatch, Faraday's rotation, and so forth. Performance-enhancing by introducing circular polarization of the MIMO antenna was discussed in Reference 21. A circularly polarized (CP) Rectenna was discussed in Reference 22 for harmonic suppression. A dual-polarized triple-band multi-beam MIMO antennas for WLAN/WiMAX applications has been implemented with almost 20 dB isolation.[23] Few UWB-MIMO antenna having circular polarization has been proposed in the existing literature like four G-shaped monopoles elements having an I-shaped strip incorporated between the ground planes to achieve a wideband 3 dB axial-ratio-bandwidth (ARBW) of 67.7% (4.2–8.5 GHz), which is suitable for C-band applications and in another case four identical square-shaped antenna elements having a circular slotted ground plane achieved a circularly polarized band from 3.8 to 6.5 GHz using a protruding hexagonal stub from the ground plane.

In some cases, an eight elements triple-band covering UWB band polarization diversity MIMO antenna has been reported for the vehicular network.[24] A compact triple-band MIMO antenna has been discussed in Reference 25 for WiMAX (2.5/3.5/5.5 GHz)/WLAN (2.4/3.6/5.8 GHz) wireless applications. Slot-based four elements reconfigurable MIMO antenna integrated with a UWB sensing antenna has been presented in Reference 26 for the cognitive radio (CR) applications.

Few 3-dimensional UWB-MIMO antennas have been designed with high isolation[27–29] among antenna elements due to their different orientation approach which gives them spatial diversity without any help of isolation techniques but the only disadvantage has been the

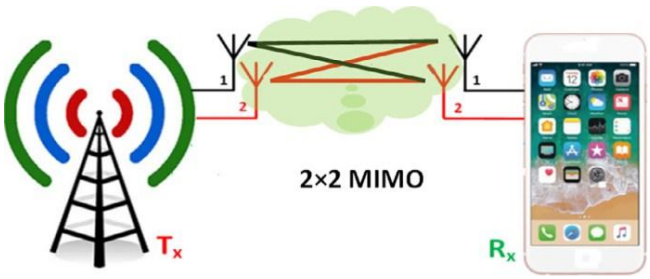

FIGURE 1 A pictorial view of 2 2 MIMO antenna system

2.1. MIMO Antenna Design Procedure

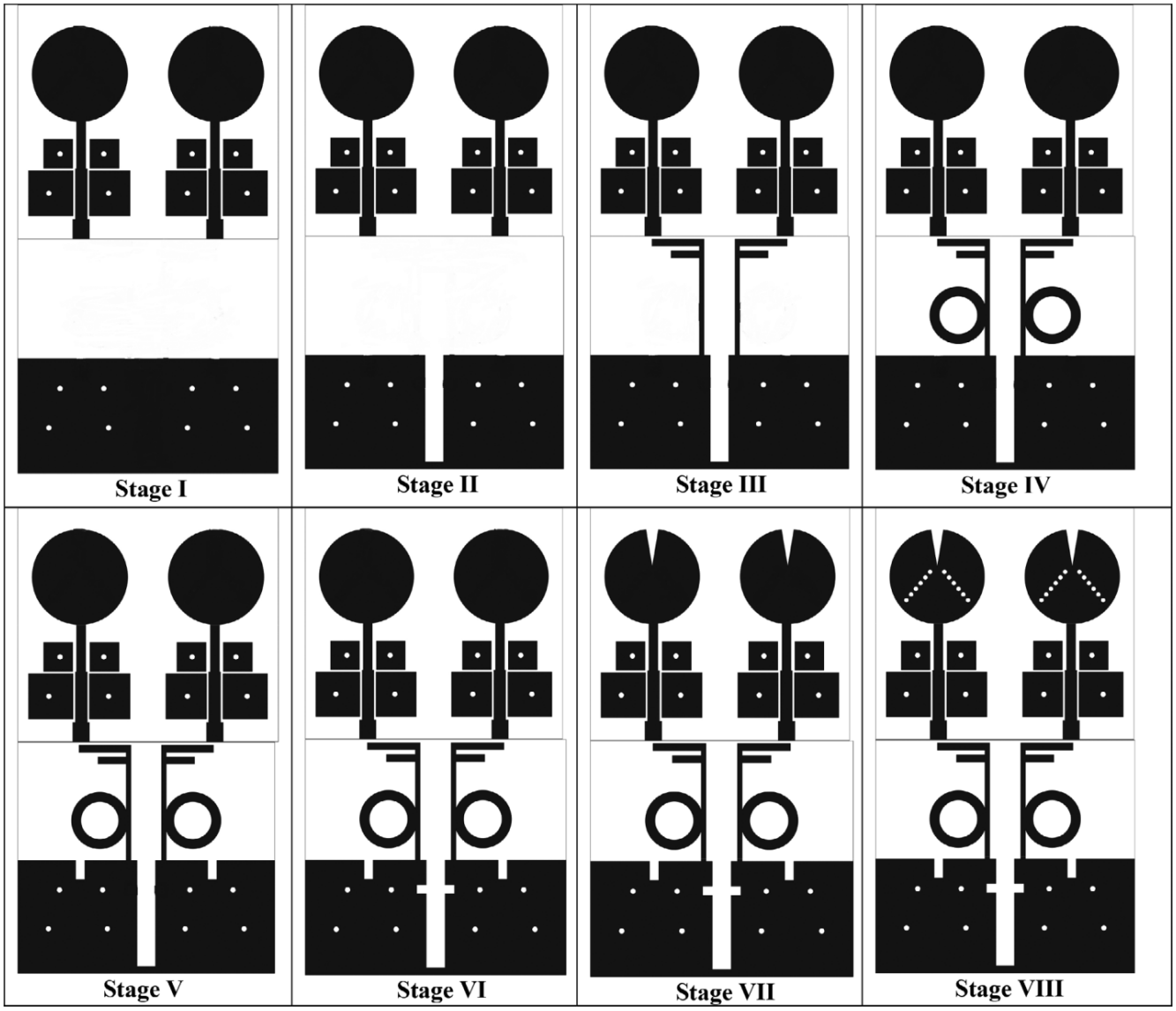

FIGURE 2 Different stages of the design of the proposed SWB-MIMO antenna

absence of common ground plane required for common reference voltage and easy integration with any device. Many Super-wideband (SWB) MIMO antennas have been recently reported like Feather-shaped SWB-MIMO antenna with no common ground resulted in high isolation of 15 dB even with a small footprint antenna area[30] while in another case tapered feed line technique has been employed to enhance the impedance bandwidth and T-shape corrugated strip has been placed among SWB-MIMO antenna elements to achieve high isolation of 20 dB.[31] A triple band-notch four-port truncated–semi-elliptical–self-complementary (TSESC) radiating patches-based SWB-MIMO antenna has been implemented in Reference 32. The notches have been achieved with the introduction of CSRR and an L-shaped slit on the patch antenna. In another SWB-MIMO antenna isolation of almost 55 dB has been achieved by a decoupling protruding ground stub.[33]

From the above discussion, we can identify that MIMO antennas are required for high-data-rate wireless transmission without sacrificing additional bandwidth. Achieving high isolation among antenna elements is another major concern especially for UWB or SWB-MIMO antennas.[1,2] A circularly polarized antenna having low SAR will be more useful to prevent signal dropout in a rich scattering especially for handheld devices and low SAR prevents health hazards. Polarization purity and SAR were discussed in Reference 34 for mobile and satellite communication.

In this paper, we have tried to give a solution to all the problems stated in the above paragraph. We have proposed an SWB quad-band circularly polarized MIMO

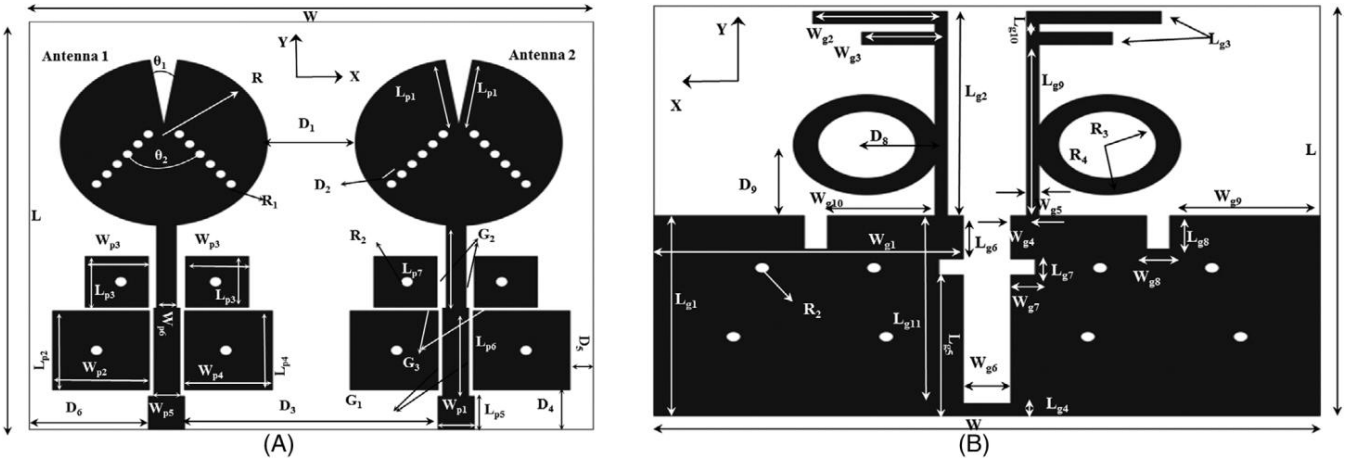

FIGURE 3 Two-element SWB planar monopole MIMO antenna: (A) Front sight; (B) Bottom sight

antenna (2.6–55 GHz) designed on a commercially available substrate FR-4 with significant results. But we have emphasized the band up to 22 GHz as the efficiency becomes poor beyond this range. Designed SWB-MIMO antenna maintaining a low specific absorption rate (SAR) due to the introduction of four electromagnetic band-gap (EBG) cells along the stepped microstrip feed line. A novel protruding F-shaped ground stub embedded with circular rings helps to achieve minimum isolation of 17 dB (20 dB at significant places) throughout the operating frequency range. Horizontal and vertical slots in the ground plane along with a V-shaped slot and six pairs of circular slots on the patch antenna helps in redistributing the current density for achieving circular polarization at 5.2/11.5/14.66/16.75 GHz. In Section 2, an antenna design procedure is explained step-by-step for SWB characteristics with quad-band circular polarization. Section 3 demonstrates the antenna results like impedance bandwidth, isolation, gain, and axial ratio. Section 4 depicts the diverse performance of the antenna in terms of envelope correlation coefficient (ECC), diversity gain (DG), total active reflection coefficient (TARC), channel capacity loss (CCL), multiplexing efficiency, channel capacity, and mean effective gain (MEG). This SWB-MIMO antenna has been simulated using the computer simulation technology-CST microwave studio simulation tool.

2 | ANTENNA DESIGN AND ANALYSIS

2.1 | MIMO antenna design procedure

The entire process of designing the proposed SWB-MIMO antenna is done from Stage I to VIII as shown in Figure 2. The proposed monopole MIMO antenna has two circular radiating patches fed by a stepped impedance microstrip line to achieve SWB characteristics. Four EBG cells of different dimensions have been introduced across the feed line for maintaining the low SAR and increasing the efficiency of the proposed MIMO antenna as depicted in Stage I of Figure 2. A big U-shaped slot (Stage II) is introduced in the center of the partial ground to reduce the mutual coupling, which is further reduced by adding a pair of F-shaped stubs (Stage III) embedded with circular rings (Stage IV), protruding from the ground plane. A couple of vertical (Stage V) and horizontal U-shaped slots (Stage VI) have been introduced in the ground plane to achieve circular polarization (CP) at 5.2 GHz. Further, a pair of V-shaped slots (Stage VII) have been added on the circular patch to deliver another CP at 11.5 GHz. Lastly, the width of the centered big-U-shaped slot in the ground plane has been optimized, and pairs of six circular slots (Stage VIII) have been introduced on the circular patch to achieve two CPs at 14.66 and 16.75 GHz. The detailed explanation of the evolution of the ground plane for the Stages I-IV has been explained in Section 3.1. Further, the Stages V–VIII are discussed in detail in Section 3.2 depicting the evolution of quad-band circular polarization. The proposed MIMO antenna is fabricated on an FR4 substrate of height, $h = 1.6$ mm, relative permittivity (ε_r) of 4.4, and loss tangent ($\tan\delta$) of 0.02.

The dimension of the antenna is 49 54.5 1.6 mm^3, as shown in Figure 3A–B. Initially, a partial ground plane of size, L_{g1} W, has been introduced to have a monopole antenna with a broader impedance bandwidth. The fundamental resonance frequency (f_{res}) of a circular-shaped monopole antenna is ¼ c= 2R ε_r p fff, where R is the radius of the antenna, ε_r is the effective dielectric constant, and c is the velocity of light (3 10^8 m/sec) in free space. At resonant frequency 10 GHz [(22–2)/2 = 10 GHz],

TABLE 1 List of antenna dimensional parameters

Parameters	L	W	L_{p1}	L_{p2}	L_{p3}	L_{p4}	L_{p5}	L_{p6}
Unit (mm)	49	54.5	8.02	9.5	6.1	9.5	4	10.6
Parameters	L_{p7}	W_{p1}	W_{p2}	W_{p3}	W_{p4}	W_{p5}	W_{p6}	L_{g1}
Unit (mm)	9.93	3.5	9.35	6.1	8.5	2.5	1.9	24
Parameters	L_{g2}	L_{g3}	L_{g4}	L_{g5}	L_{g6}	L_{g7}	L_{g8}	L_{g9}
Unit (mm)	24.5	1.5	1.5	16.9	5.2	1.9	4	20.5
Parameters	L_{g10}	L_{g11}	W_{g1}	W_{g2}	W_{g3}	W_{g4}	W_{g5}	W_{g6}
Unit (mm)	1	22.5	25.3	11	7	1.3	1	3.9
Parameters	W_{g7}	W_{g8}	W_{g9}	W_{g10}	R	R_1	R_2	R_3
Unit (mm)	2	1.9	12.3	8.8	10	0.5	0.6	4
Parameters	R_4	G_1	G_2	G_3	D_1	D_2	D_3	D_4
Unit (mm)	6	0.45	0.85	0.45	8.54	1.76	23.5	4.75
Parameters	D_5	D_6	D_7	D_8	D_9			
Unit (mm)	2.65	12	2.65	6.5	8.5			
Angle	θ_1	θ_2						
Degree	18.92	100						

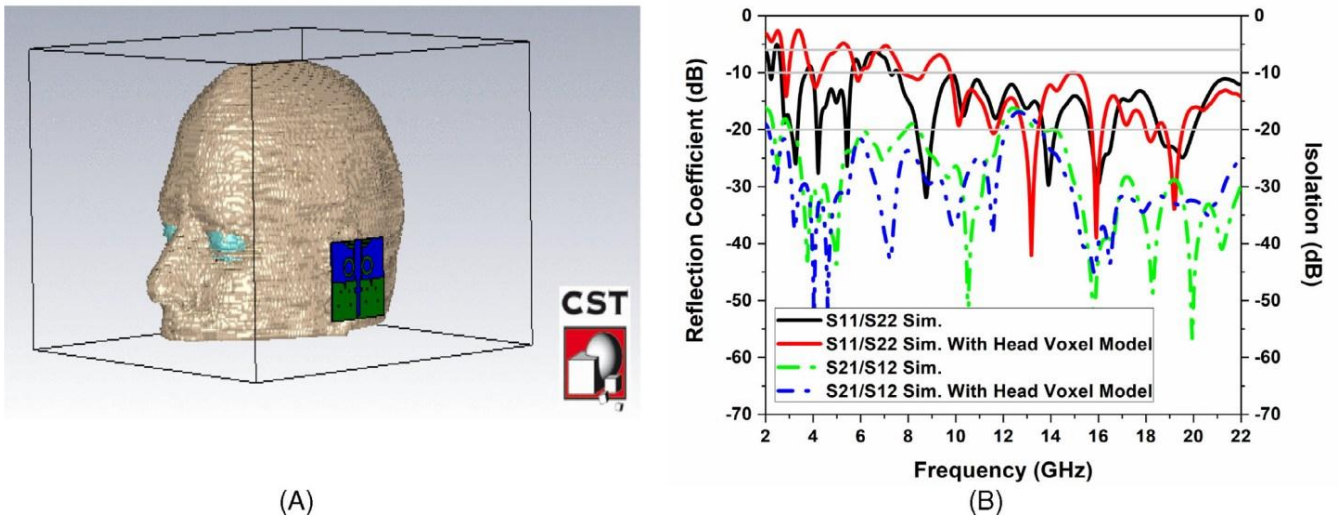

FIGURE 4 (A) Representation of the proposed MIMO antenna with head voxel model; (B) S-parameters analysis with and without head voxel model

the value of R is approximately 10 mm as calculated by using Equation (1).

$$R = \frac{18412c}{2\pi f_r \sqrt{\varepsilon_{eff}}} \quad (1)$$

We have taken a circular patch antenna of radius R = 10 mm, which is fed by a stepped impedance line of length (L_{p5} + L_{p6} + L_{p7}) = 24.53 mm to have a wide impedance bandwidth ranging from 2.6 to 22 GHz. Here we show the effective impact of the stepped impedance of the microstrip feed line. If we merged 50 Ω, 63 Ω, and 73 Ω impedance lines, it shows like a triangular tapered line for providing maximum power to the radiator in an SWB. The input impedance of the radiator is approximate 73 Ω then we calculate the characteristics impedance of the middle microstrip feed line which is about 63 Ω by using the formula $Z_0 = \sqrt{Z_{in} Z_1} = \sqrt{50 \times 73} \approx 63\ \Omega$ which provides maximum power ports to the radiator.[35] We have introduced an inverted F-shaped protruding ground stub embedded with a circular ring and a large U-shaped slot cut of dimension L_{g11} W_{g6} in the center of the monopole ground for achieving high isolation by diverting and

providing an additional decoupling path to the surface current before reaching the adjacent antenna element.

Four EBG cells of different dimensions have been introduced across the feed line for maintaining the low SAR and increasing the efficiency of the proposed MIMO antenna. The complete analysis of EBG has been explained later on in this section. Various U-shaped slots have been etched in the ground to redistribute the surface current equally in the vertical and horizontal direction to achieve circular polarization in the 5.2 GHz WLAN band. V-shaped slot etched and a pair of six circular cuts in the patch for achieving circular polarization at 11.50 GHz, 14.66 GHz, and 16.75 GHz. $\theta_1 = 18.92$ is the final value of θ_1 varying it to an interval of 1 which finally ends at 18.92 to achieve CP at 11.5 GHz. Similarly, the final $\theta_2 = 100$ is the result of variation of angle θ_2 at an interval of 20 which finally ends with 100 where we got the intended results. The detailed antenna parameters have been tabulated in Table 1. All the antenna parameters have been optimized using the CST simulation tool for better results.

2.2 | EBG analysis and its significance

EBG plays a significant role in increasing the front-to-back ratio (FBR) and maintaining the efficiency of the antenna in a lossy dielectric substrate. We can find significant contributions of EBG in the existing literature like helpful in creating band-notch,[36] isolation enhancement, enhancing antenna characteristics like gain & bandwidth,[37] and improving FBR.[38,39] The center frequency of the proposed mushroom-shaped EBG structure near the feed line is calculated by Equation (2).[39]

$$f_{EBG} = \frac{1}{2\pi \sqrt{L_{eq}\left(C_{gap\ eq} + C_{plate\ eq}\right)}} \quad (2)$$

Gap capacitance ($C_{gap\ eq}$), plate capacitance ($C_{plate\ eq}$), and lumped inductance (L_{eq}) are calculated by an equation that is depicted in Reference 39. The resonant frequency is coming out to be 21.24 GHz from the equivalent circuit model analysis explained in Reference 39. While 23.78 GHz as calculated by Equation (1), indicates the importance of EBG cells in retaining efficiency at higher resonant frequencies in a lossy dielectric substrate like FR-4.

2.2.1 | Specific absorption rate (SAR)

SAR has been calculated for the proposed MIMO antenna by placing it at a distance of 10 mm from the head voxel model, as represented in Figure 4A. The computed maximum SAR is coming out to be 1.095 W/kg at 3.5 GHz, which is way below the recommended SAR limit of 2 W/kg[38–40] average over 10 g of head bio tissue. We have given a simulated input power of 0.5 W, of which the accepted power is 0.318 W. We have also calculated the SAR value without EBG cells, and the value increases to 1.753 W/kg at 3.5 GHz. While the situation without EBG is even

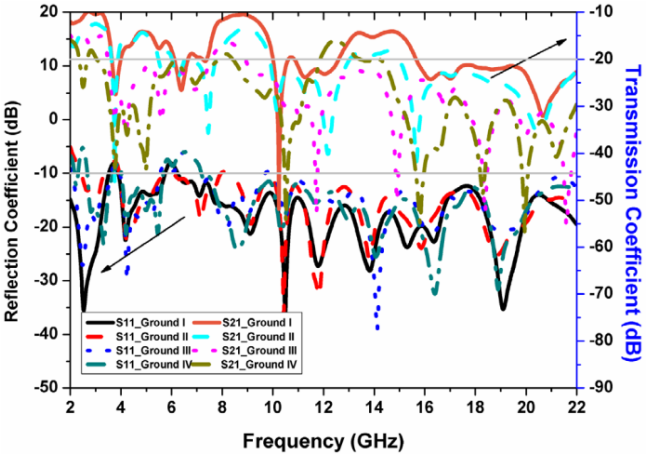

FIGURE 6 Simulated S-parameters analysis of the different Grounds I–IV given in Figure 5

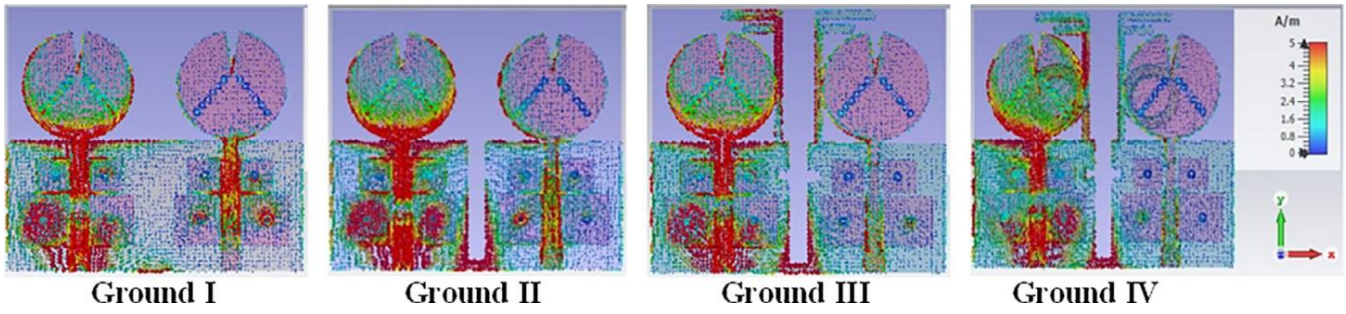

FIGURE 5 Surface current distribution in the proposed MIMO antenna for different grounds (I–IV) at 3 GHz resonant frequency

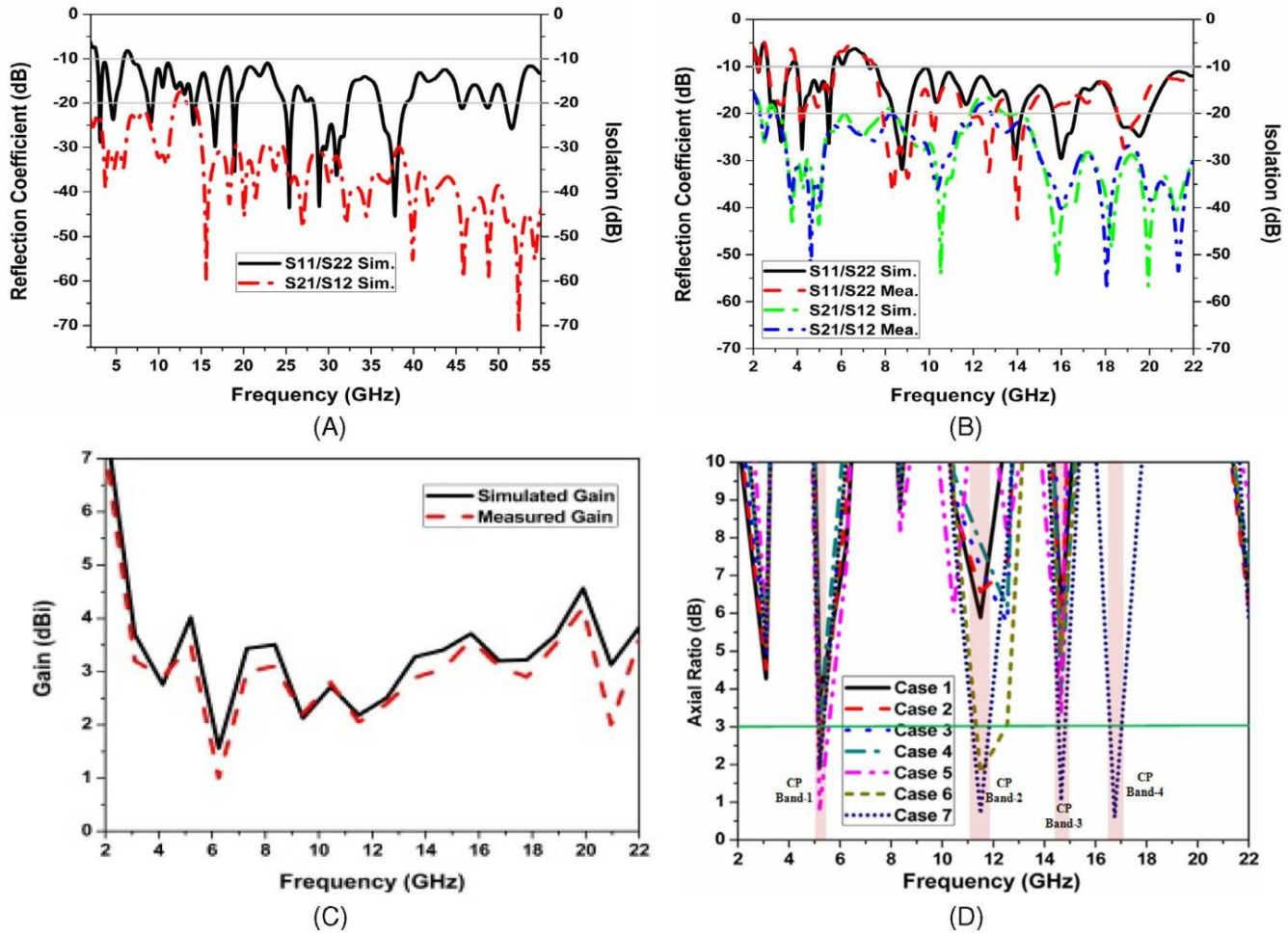

FIGURE 7 (A) Simulated S-parameter for SWB; (B) simulated and measured S-parameters for claimed working range gain (2.6–55 GHz); (C) gain versus frequency; and (D) quad-band axial ratio versus frequency

worse at higher frequencies, say around 20 GHz. Although SAR is of not much significance at higher frequencies as far as the human body is concerned, we like to highlight and conclude that the EBG cells will help to retain the efficiency as well the SAR value within the limit at these high frequencies too. The simulated S-parameters results with and without head voxel model have been described in Figure 4B where we can observe that the variation in the reflection coefficient is acceptable taking into consideration the 6 dB threshold for the MIMO antenna like many others[15,41] except some higher variation around 3.5 GHz. The efficiency is as high as 80% for the proposed MIMO antenna around 3.5 GHz without voxel model but has gone down to 65%–70% with the head voxel model which is still in good considerations taking the MIMO antenna effect into the account for high data rate transmission.

3 | RESULTS AND DISCUSSION

3.1 | S-parameters and ground plane analysis

First of all, we will discuss the various defected ground structures (DGSs) introduced step by step for achieving the desired isolation of 20 dB for a significant part of the claimed SWB (2–22 GHz). We have divided the iterations into four Grounds (I–IV) along with the surface current distribution at one of the resonant frequencies 3 GHz for demonstration, as shown in Figure 5. We can see how the concentration of surface current density on another monopole antenna due to the excitation of the first monopole antenna is decreasing as preceding from Ground-I to IV. Firstly the major part of the surface current was accumulated around the curve of the large U-shaped cut in Ground-II. Then some portion is

TABLE 2 Effects on ARBW in different cases with the specific method applied

Case	Figure 2 correspondent Shape only	Variation in length and width of the three U-shaped slots (mm)			Method applied	ARBW range/ BW (GHz)	Min AR Freq. (GHz)/ Value (dB)
		L_{g8}	W_{g7}	W_{g6}			
1	Stage V	3	0	4.7	Two small vertical U-shaped slots (L_{g8} W_{g8})	Nil	Nil
2	Stage V	3.5	0	4.7	Case 1	5.18–5.30/0.120	5.2/2.33
3	Stage V	4	0	4.7	Case 1	5.18–5.32/0.145	5.2/2.07
4	Stage V	4.5	0	4.7	Case 1	5.15–5.25/0.100	5.2/2.33
5	Stage VI	4	4	4.7	Case 1 + Horizontal U-shaped slots (L_{g7} W_{g7})	5.13–5.56/0.430	5.2/0.82
6	Stage VII	4	2	4.7	Case 5 + V-shaped Slot in the circular patch	5.16–5.34/0.180, 11.32–12.52/1.2	5.2/2.05, 11.5/1.77
7	Stage VIII	4	2	3.9	Case 6 + Reduced width of largest U-shaped slot (L_{g11} W_{g6}) + a pair of six circular slots in the circular patch	5.16–5.34/0.180, 11.15–11.85/0.700, 14.54–14.83/0.300, 16.53–17.03/0.500	5.2/1.90, 11.50/0.70, 14.66/1.05, 16.75/0.61

distributed along with the F-shaped stubs in Ground-III, which was further supported by the circular rings attached to the F-shaped stubs in Ground-IV, resulting in the elimination of high density of surface current majorly available around the feed line and EBG area of the second monopole as shown in Ground-I of Figure 5. The same results can be verified with the simulated S-parameters analysis presented in Figure 6. We can observe from Figure 6 that the transmission coefficient was above 10 dB for Ground-I at 3 GHz, which was improved to 13 dB in Ground-II, then 16 dB in Ground-III, and finally below 20 dB in Ground-IV. A similar kind of improvement in the transmission coefficient can be observed at 5 GHz and 9 GHz without causing much disturbance to the reflection coefficients throughout the SWB. A slight disturbance in the reflection coefficient is observed around 6–7 GHz due to various iterations involved for achieving significant isolation, but still, the value is below 6 dB, which can be considered in a MIMO antenna system.[15,41]

Measured and simulated results of the proposed SWB-MIMO antenna like return loss, isolation, peak gain, and the axial ratio is represented in Figure 6A–C. We have shown the S-parameters for the entire operating band ranging from 2 to 55 GHz in Figure 7A, but as the efficiency decreases drastically from 80% to 45% after 22 GHz, so we have restricted our observations up to 22 GHz only, see Figure 7B–D. We can observe minimum isolation of 17 dB (20 dB for the significant part) in the simulated and measured result as well in Figure 7B. Gain is varying from 1.5 to 4.58 dBi as shown in Figure 7C. The measured axial-ratio of the proposed MIMO antenna at 5.2, 11.50, 14.66, and 16.75 GHz is less than 3 dB, which indicates that the antenna is circularly polarized, as shown in Figure 7D. Mobile phones and other movable handheld devices antenna required at least half-power in every plane for the useful communication link, so circular polarization of this antenna is helpful for various wireless applications.

3.2 | Circular polarization analysis

The whole iteration cases from 1 to 7 to achieve circular polarization have been tabulated in Table 2. The design procedure can be verified from the Stages V to VIII shown in Figure 2. The Stages V–VIII shown in Figure 2 is only for shape analysis of different cases from 1 to 7. Stage V corresponds to cases 1 to 4, Stage VI corresponds to case 5, Stage VII corresponds to case 6, and Stage VIII corresponds to case 7 which are tabulated in Table 2. Firstly in case 1, two vertical U-shaped slots of dimensions, L_{g8} W_{g8}, have been introduced,

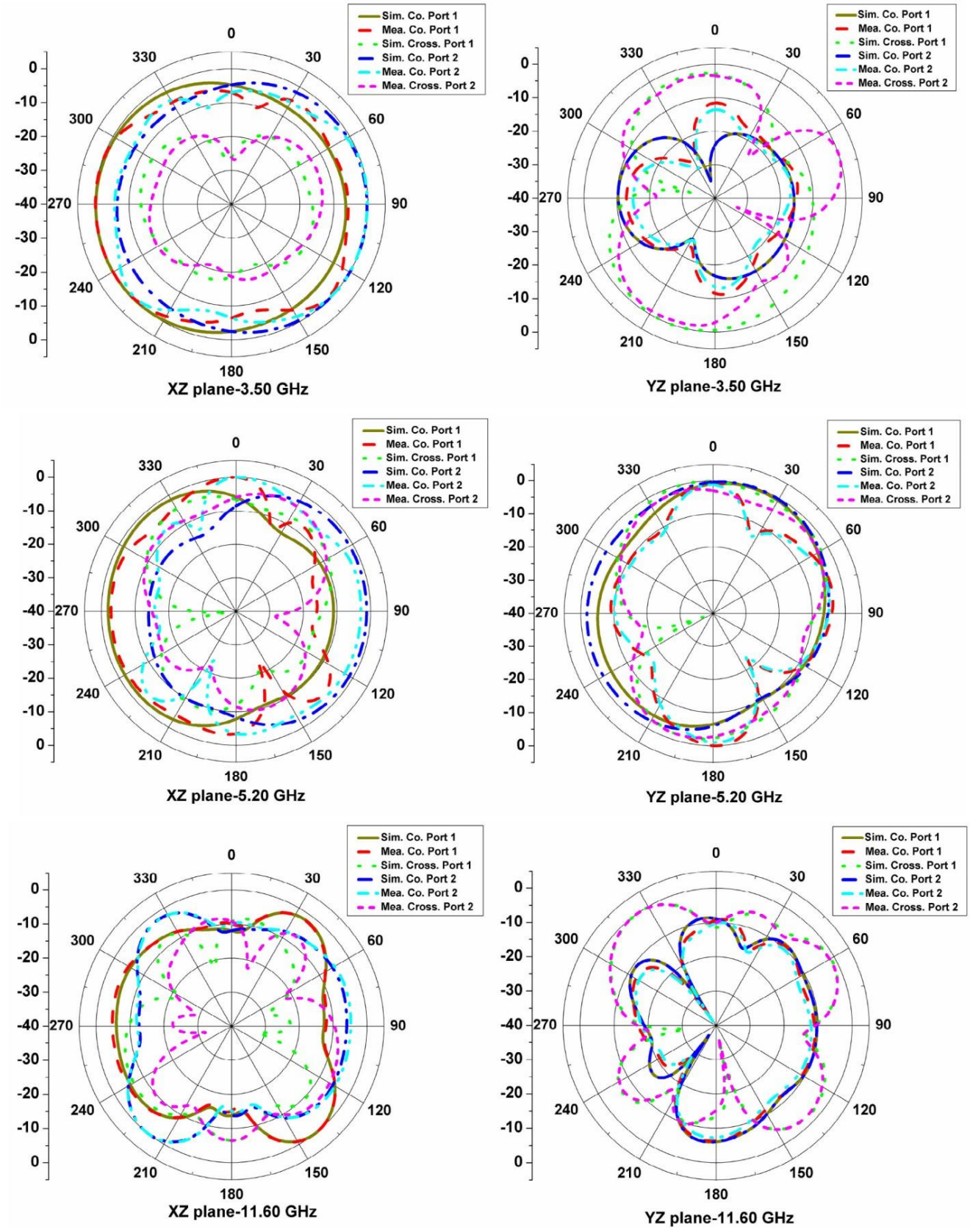

FIGURE 8 Measured & simulated 2D radiation patterns at 3.5, 5.2, 11.6, 14.66, 16.75, and 20 GHz for XZ-plane and YZ-plane

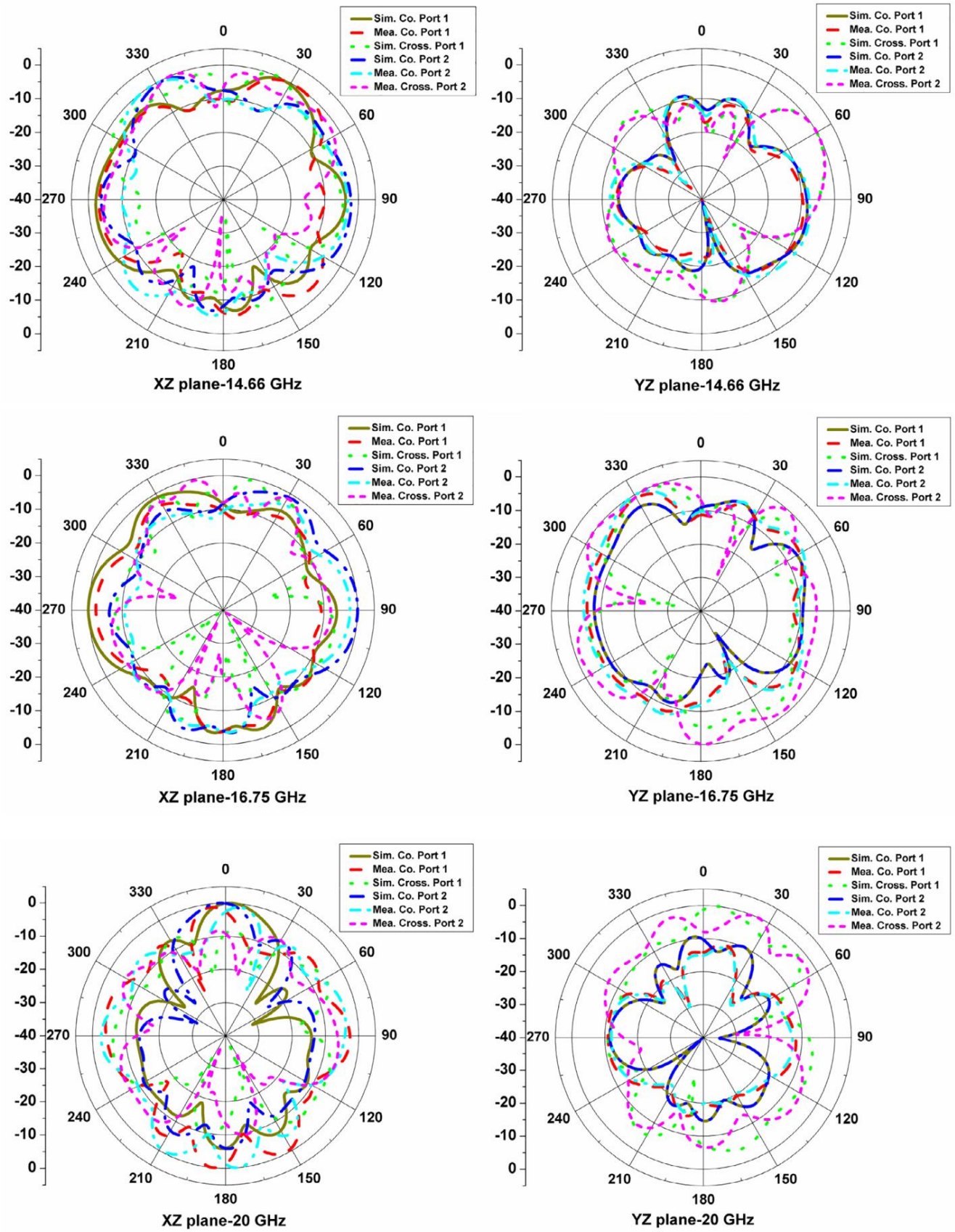

FIGURE 8 (Continued)

but no axial-ratio-bandwidth (ARBW) has been achieved as depicted in Figure 7D. The length of the vertical U-shaped is varied from 3.5 to 4.5 mm, which resulted in significant improvement in ARBW at 5.2 GHz till cases 2 & 3 and a drop in ARBW in case 4 so, we restrict ourselves with L_{g8} = 4 mm. Now in case 5, we introduced a horizontal U-shaped slot of dimension L_{g7} W_{g7}, which shows a significant rise of ARBW to 430 MHz centered at 5.2 GHz, with an excellent axial-ratio of 0.82 dB. In case 6, we have introduced a V-shaped slot cut on the circular patch of length L_{p1}, which gives an excellent ARBW of 1.2 GHz at 11.5 GHz. Lastly, in case 7, the width of the largest centered U-shaped slot W_{g6} has been optimized to 3.9 mm from 4.7 mm along with the introduction of a pair of six circular cuts in the circular patch, which helps in improving and hence achieving the ARBW of 300 MHz at resonant frequency 14.66 GHz and achieving another ARBW of 500 MHz at 16.75 GHz. The above-mentioned circular polarization with significant ARBW makes our antenna widely accepted for C-band, X-band, and Ku-Band wireless applications.

3.3 | Radiation pattern analysis

The radiation distinctiveness of the MIMO antenna is investigated in SWBs. For the measurements of antenna one, the other another antenna is terminated with a matched load of 50 Ω and vice-versa. Normalized radiation patterns are shown in Figure 8. When port-1 is excited, the radiating power of antenna-1 is shifted towards the left of the XZ-plane, and towards the right side for antenna-2. This will help in achieving pattern diversity in XZ-plane, which reduces the correlation among the antenna elements. The fabricated model, along with the measurement set-up, is shown in Figure 9A–C.

In Figure 8, the co-and cross-polarization effect is evident at 3.5 and 20 GHz, where the isolation is more than 20 dB in the main lobe radiation advocating linear polarization while the gap is less for the rest frequencies advocating CP at those frequencies. The same concept is strengthened by the normalized left-hand-circular-polarization (LHCP) and right-hand-circular-polarization (RHCP) radiation pattern shown in Figure 10, which shows a gap of more than 20 dB between RHCP and LHCP in the main lobe direction, advocating CP at those frequencies. When Port-1 is excited you can see that the LHCP simulated value (LHCP Sim. Port-1) is higher in the main lobe direction say at $\theta = 0^0$ for both XZ and YZ-Plane for frequencies 5.20 and 14.66 GHz claiming LHCP. Similarly when Port-2 is excited the RHCP measured value (RHCP Sim. Port-1) is higher at frequencies 11.60 and 16.75 GHz advocating RHCP. The type of polarization at different frequencies and ports is mentioned in Table 3.

The surface current distributions at the CP frequencies have been shown in Figure 11A–D for the different phases, ϕ is varying from 0^0 to 270^0 by exciting port-1, and terminating the port-2. We can see the clockwise movement of the surface current, especially around the EBG introduced area at frequencies 5.20 and 14.66 GHz claiming LHCP[42] due to port-1 excitation while an anti-clockwise movement at frequencies 11.60 and 16.75 GHz is claiming RHCP due to port-1 excitation. As stated in Table 3 the polarity changes for the Port-2 means the proposed antenna elements show RHCP at frequencies 5.2 and 14.66 GHz for Port-2 while LHCP for frequencies 11.60 and 16.75 GHz for Port-2 excitation.

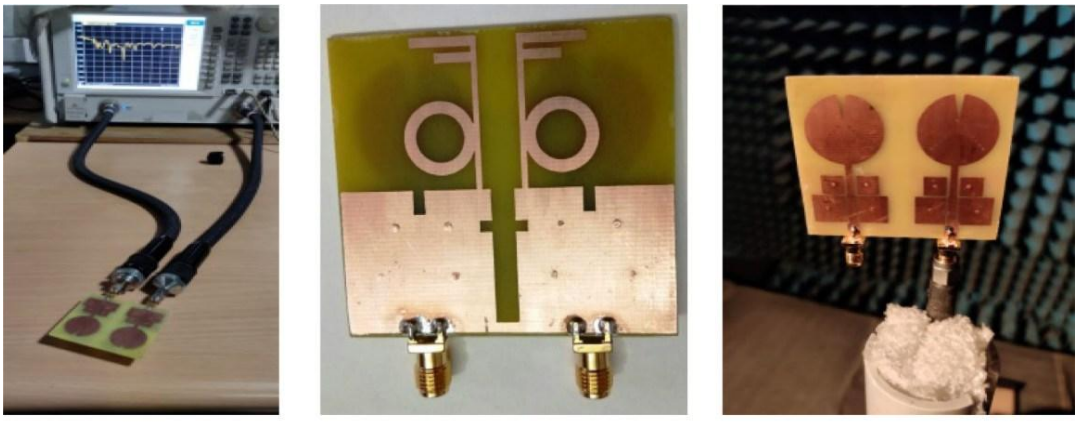

FIGURE 9 Fabricated MIMO antenna prototype: (A) front view with VNA; (B) back view; (C) anechoic chamber set-up

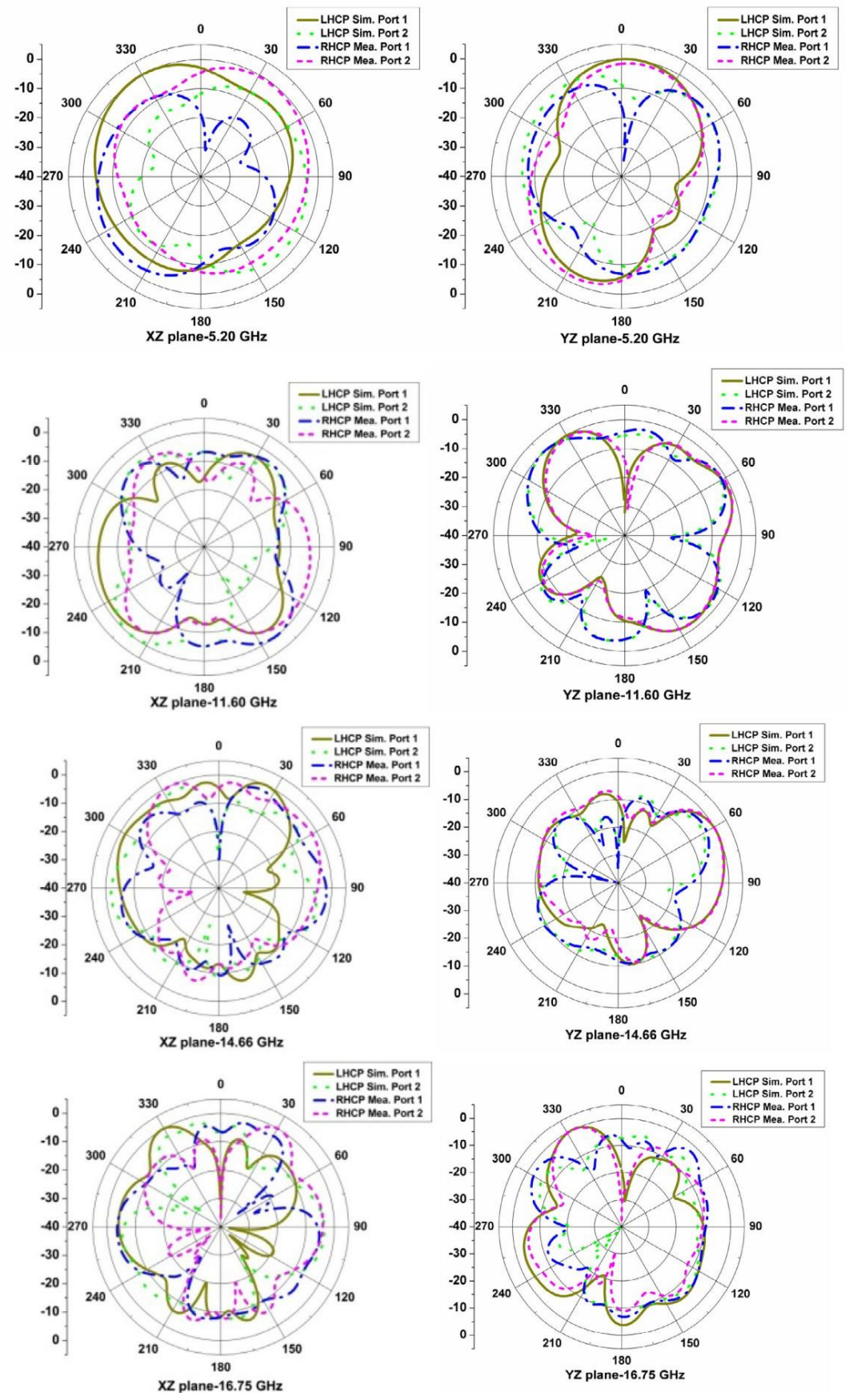

FIGURE 10 Normalized LHCP and RHCP radiation patterns at 5.2, 11.5, 14.66, and 16.75 GHz for both the ports

TABLE 3 List of polarization type at the circularly two-ports at polarized quad-bands

	Type of polarization	
Resonant frequency (GHz)	Port 1	Port 2
5.20	LHCP	RHCP
11.60	RHCP	LHCP
14.66	LHCP	RHCP
16.75	RHCP	LHCP

4 | MIMO DIVERSITY PERFORMANCE

MIMO diversity performance characteristics are evaluated to certify the performance of the proposed MIMO antenna elements without much hindrance from the neighboring elements on the same substrate along with the common ground. Each parameter is discussed in this section in detail.

4.1 | Envelope correlation coefficient (ECC) and diversity gain (DG)

ECC is one of the important parameters for MIMO applications, which shows how much amount of correlation between the excited antennas to the rest of the antennas. It can be calculated through S-parameters by Equation (3),[15,42] but this equation is only valid for lossless where power is uniformly distributed among antennas.

$$\rho_{ecc,ij} = \frac{\left|\sum_{n=1}^{N} S_{in}^{*} S_{nj}\right|^2}{\left(1-\sum_{n=1}^{N}|S_{ni}|^2\right)\left(1-\sum_{n=1}^{N}|S_{nj}|^2\right)} \quad (3)$$

We can have the more reliable computation of the ECC of the MIMO antenna by Equation (4)–(5)[39,43] in terms of radiated fields.

$$\rho_{ecc,ij} = \frac{\left|\int_0^{2\pi}\int_0^{\pi}\left[XPR\,E_{\theta i}(\theta,\phi)E_{\theta j}(\theta,\phi)P_{\theta}+E_{\phi i}(\theta,\phi)E_{\phi j}(\theta,\phi)P_{\phi}\right]d\Omega\right|^2}{\int_0^{2\pi}\int_0^{\pi}\left[XPR\,G_{\theta i}P_{\theta}+G_{\phi i}P_{\phi}\right]d\Omega \int_0^{2\pi}\int_0^{\pi}\left[XPR\,G_{\theta j}P_{\theta}+G_{\phi j}P_{\phi}\right]d\Omega} \quad (4)$$

$$\rho_{ecc,ij} = \frac{\left|\int_0^{2\pi}\int_0^{\pi} E_i(\theta,\phi)E_j(\theta,\phi)d\Omega\right|^2}{\int_0^{2\pi}\int_0^{\pi}|E_i(\theta,\phi)|^2 d\Omega \int_0^{2\pi}\int_0^{\pi}|E_j(\theta,\phi)|^2 d\Omega} \quad (5)$$

For uncorrelated MIMO antenna, ECC is zero, but their acceptable practical value for practical MIMO antenna is ≤0.5. In Figure 12A, the ECC (radiated field) of the proposed MIMO antenna in SWB is observed using Equation (4) which is coming less than 0.05, which depicts excellent diversity performance. Another critical parameter is diversity gain; the diversity gain (DG) is the increase in signal-to-interference ratio due to some diversity scheme. The diversity gain of the MIMO antenna is calculated by $DG = 10\sqrt{1-ECC^2}$,[44] for satisfactory operation of the MIMO antenna, diversity gain (DG) should be >9.5 dB. The dB value of DG in SWB is >9.98 dB, which is depicted in Figure 12A.

4.2 | Channel capacity loss (CCL)

The main aim of using the MIMO antenna is to enhance channel capacity. More elements advocate large channel capacity, but the correlation among these elements results in losses, which is termed channel capacity loss (CCL), and it is calculated by Equations (6)–(8) presented in Reference 15. CCL from simulated and measured are shown in Figure 12B. The CCL value in the intended operating bands is below the prescribed value. Ideally, zero correlation provides zero channel capacity loss, but its practical value is <0.4 bps/Hz for MIMO antenna. CCL is dependent upon S-parameters calculated by the following Equations (6)–(8).

$$CCL = -\log_2(\psi^{p}) \quad (6)$$

$$\text{Where, } \psi^{p} = \begin{vmatrix} \rho_{11} & \rho_{12} \\ \rho_{21} & \rho_{22} \end{vmatrix}$$

$$\rho_{ii} = 1-\left(\sum_{n=1}^{N} S_{in}^{*} S_{ni}\right) \quad (7)$$

$$\rho_{ij} = -\left(\sum_{n=1}^{N} S_{in}^{*} S_{nj}\right), \text{ where } i,j,n = 1,2 \quad (8)$$

Figure 12B shows the CCL, and it is less than 0.35 bits/s/Hz over the intended bandwidth, which offers a better diversity result of the proposed MIMO antenna.

4.3 | Total active reflection coefficient (TARC)

TARC is the square root of the ratio of total reflected power to the total incident power at the same port. For the n-element MIMO antenna system at the transmitter and receiver end, it can be evaluated by Equations (9)–(11).[39,43]

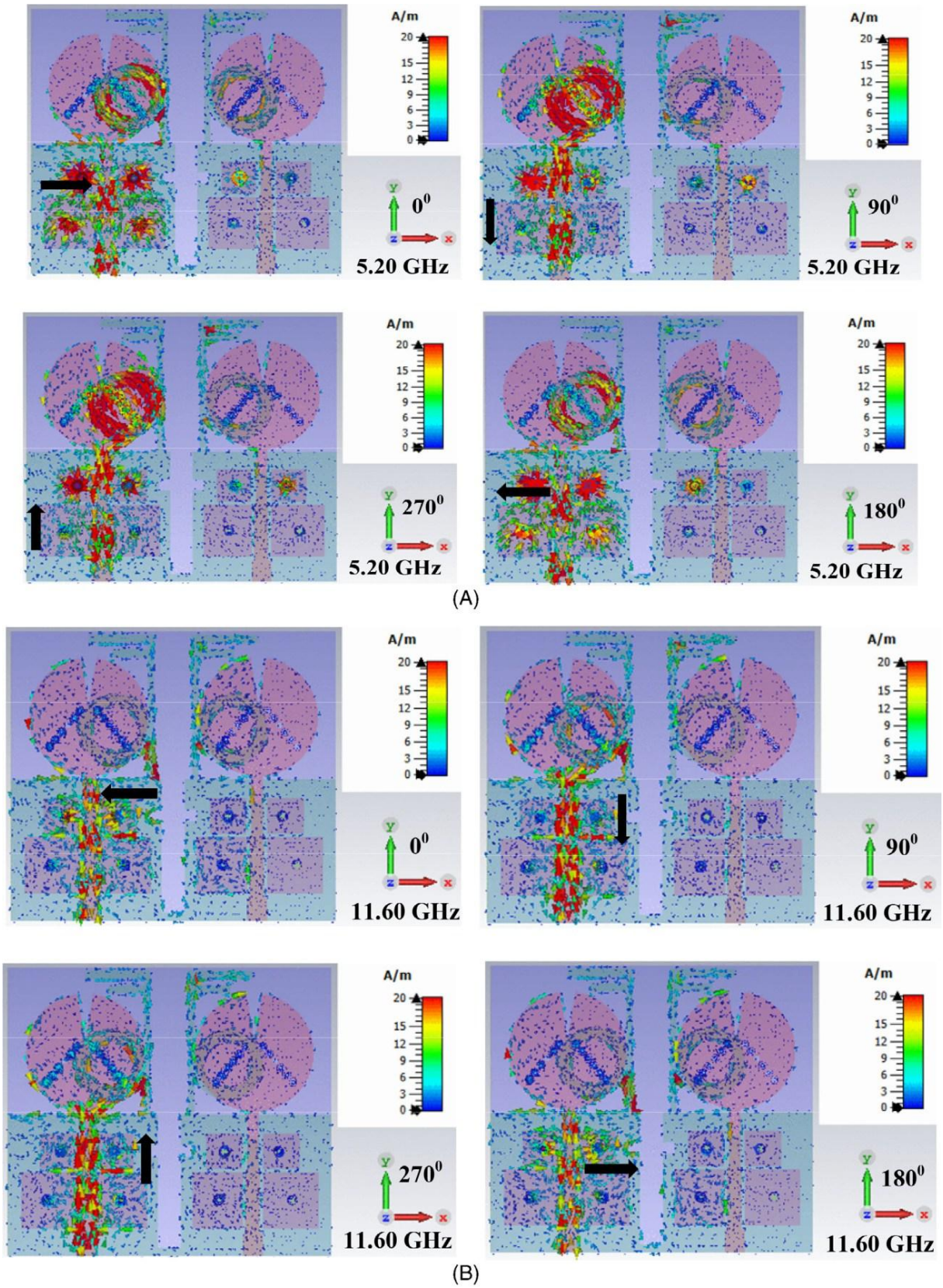

FIGURE 11 Surface current distribution at frequencies: (A) 5.2, (B) 11.6, (C) 14.66, and (D) 16.75 GHz, where ϕ is varying from 0^0 to 270^0 when antenna-1 is energized and another antenna is terminated with matched 50 Ω load

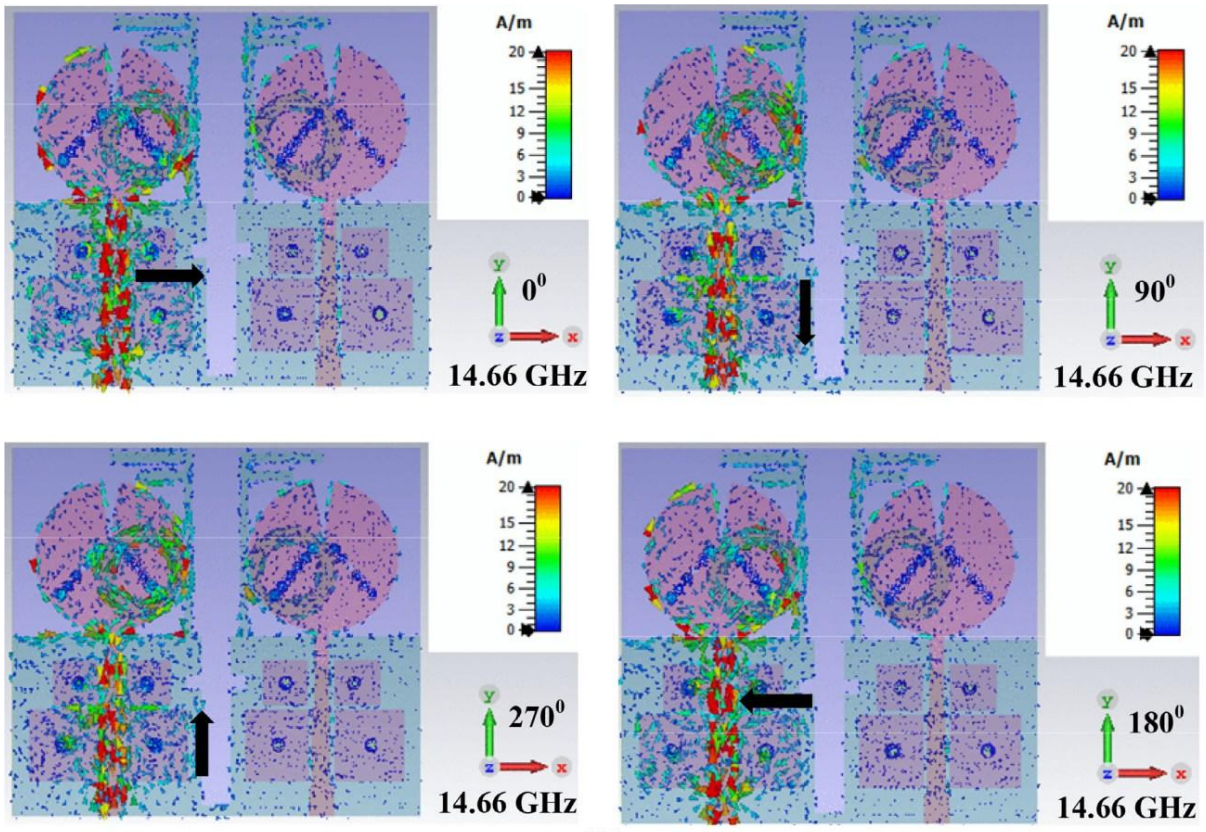

(C)

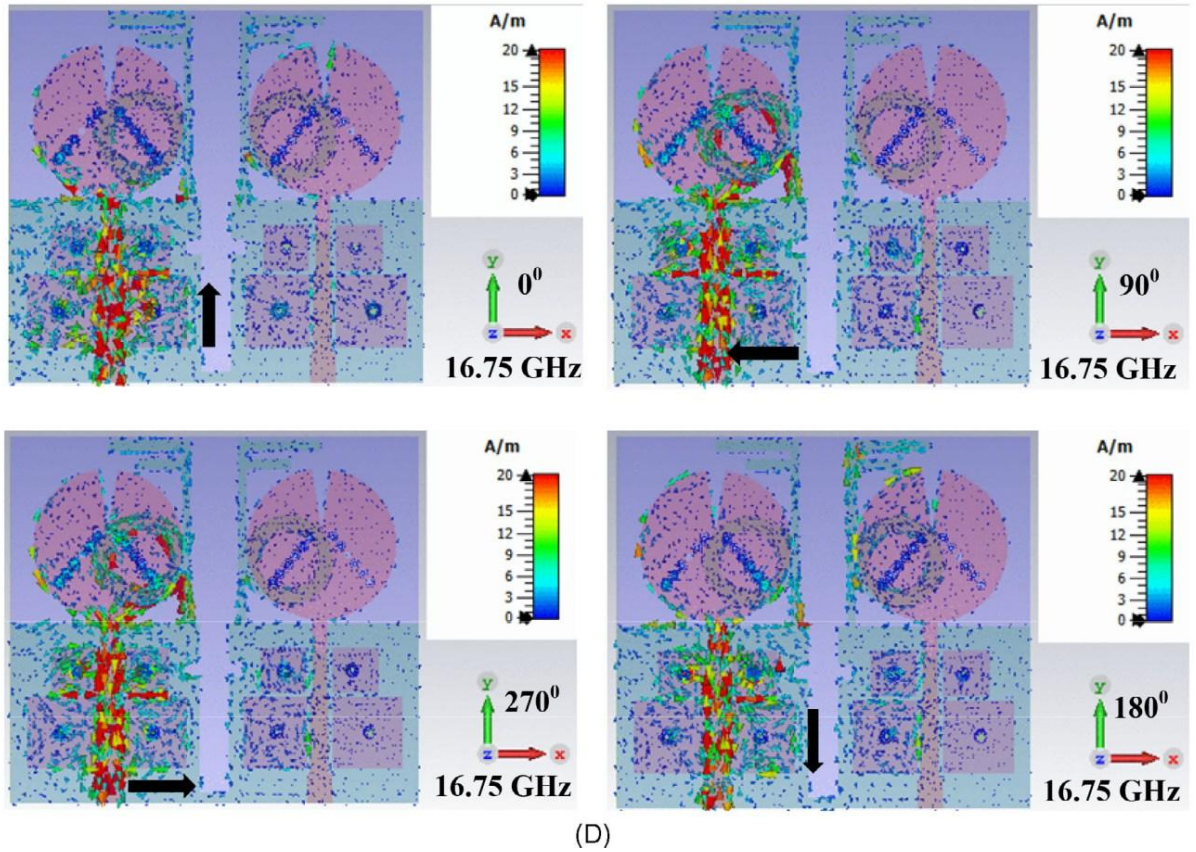

(D)

FIGURE 11 (Continued)

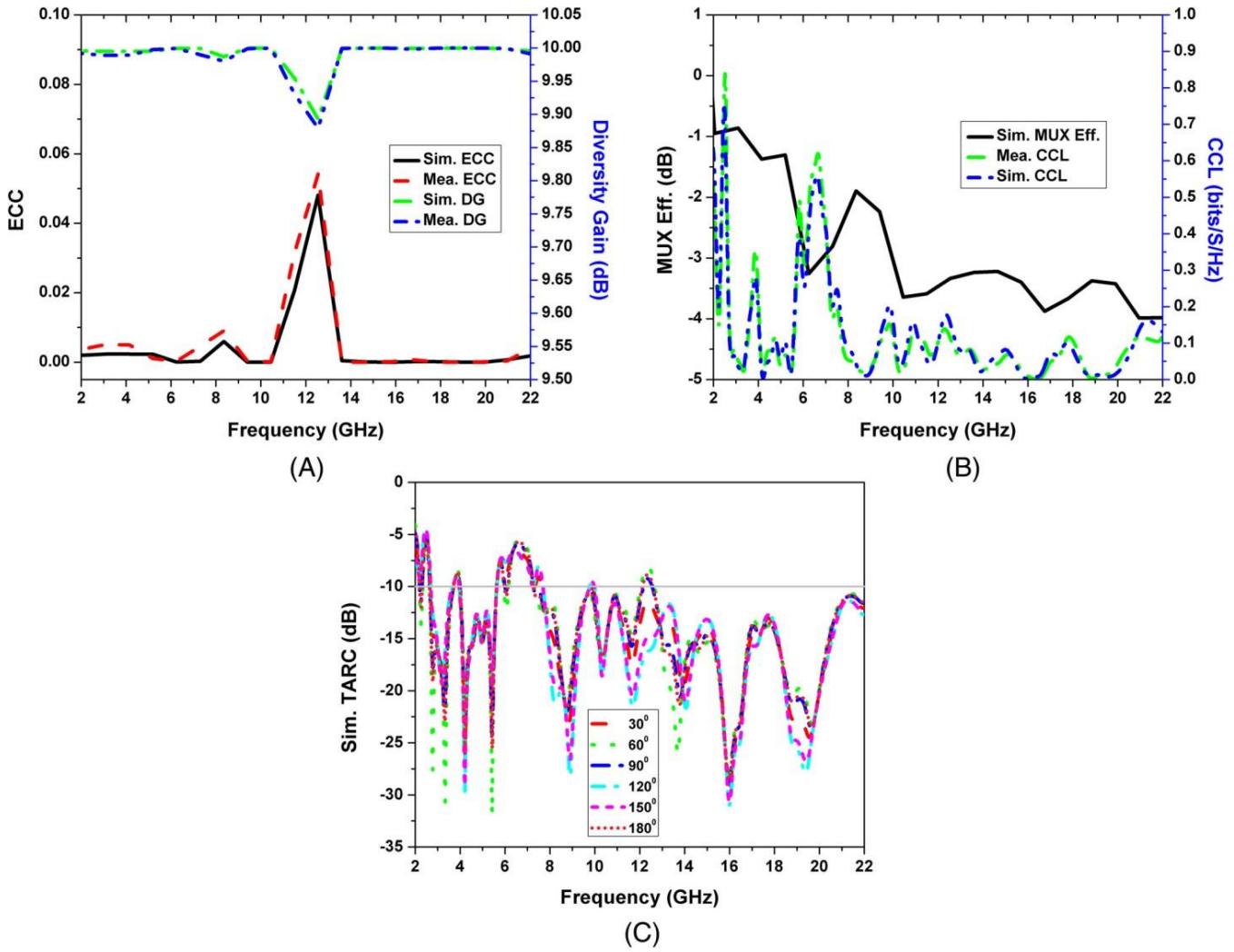

FIGURE 12 Simulated and measured results of (A) ECC and DG from radiated fields; (B) multiplexing efficiency; and CCL (C) TARC versus frequency of proposed MIMO antenna

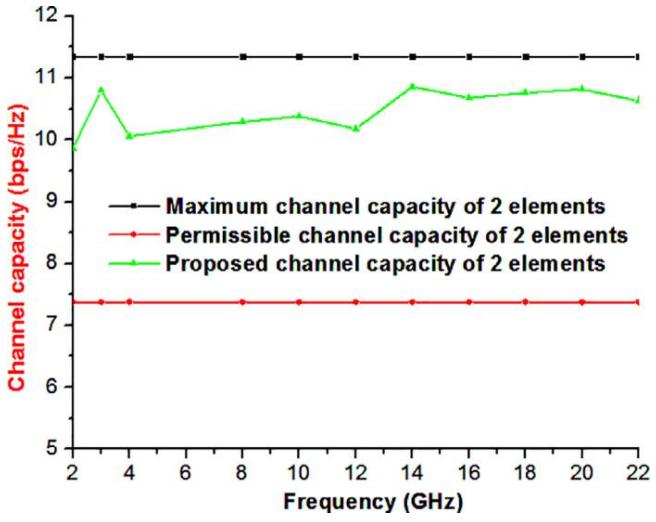

FIGURE 13 Average channel capacity of the proposed two-element array antenna system

$$\text{TARC} = \frac{\sum_{n=1}^{N} |b_i|^2}{\sum_{n=1}^{N} |a_i|^2} = \frac{\sqrt{|S_{ii} + S_{ij} e^{j\theta}|^2 + |S_{ji} + S_{jj} e^{j\theta}|^2}}{n} \quad (9)$$

where a_i and b_i is incident wave and reflected wave, respectively, and n denotes the number of antenna elements. θ denotes the phase change of the input signal.

$$[b] = [S][a] \quad (10)$$

where [S], [a] and [b] are scattering, incident and reflected matrix, respectively. So, for a 2 2 MIMO antenna the TARC equation will be as follows:

$$\text{TARC} = \frac{\sqrt{|S_{11} + S_{12} e^{j\theta}|^2 + |S_{21} + S_{22} e^{j\theta}|^2}}{n} \quad (11)$$

TABLE 4 Simulated MEG results of proposed MIMO antenna at various frequencies

	MEG (dB)		MEG (dB)	
	Laplacian medium		Gaussian medium	
Frequency (GHz)	XPR = 1 dB	XPR = 6 dB	XPR = 1 dB	XPR = 6 dB
2.6	4.17	6.02	4.45	6.23
5.2	6.12	5.12	4.18	6.11
11.6	7.13	6.84	3.82	5.12
16.75	5.14	5.01	3.26	3.18
20	4.82	4.22	4.10	3.98

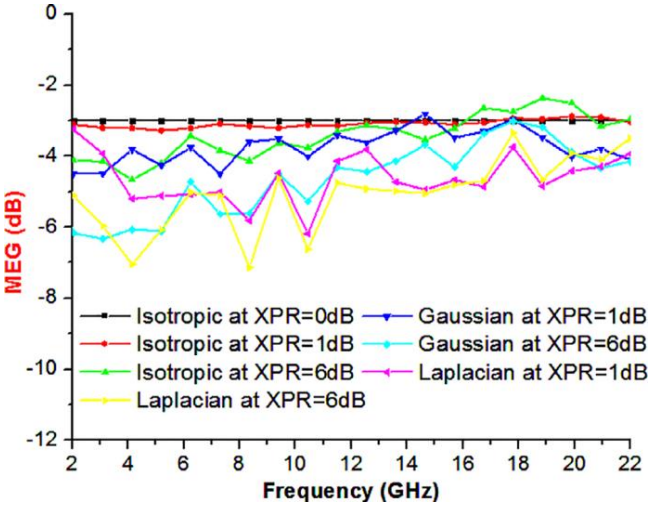

FIGURE 14 Simulated results of mean effective gain in isotropic, Laplacian, and Gaussian medium at different XPR values of the proposed antenna

Ideally, TARC should be less than 0 dB for any MIMO antenna system. The simulated and measured TARC of the designed MIMO antenna is less than 10 dB in the intended SWB shown in Figure 12C, again it shows the excellent diversity performance of a designed antenna. The phase of the input signal is fixed for one port and changed for the other ports by 30^0 till 270^0 to observe the change in the reflection coefficient as shown in Figure 12C. We can observe from the result that the TARC is following the reflection coefficient of our proposed antenna even the phase of the input signal ports is changing ensuring the good diversity performance of the antenna.

4.4 | Multiplexing efficiency

The multiplexing (MUX) efficiency of an antenna is an important parameter that does not only provide information about the total antenna efficiency but also gives them information about the efficiency imbalance in MIMO systems. It is calculated by $1 - |\rho_c|^2 \eta_i$, where ρ_c is a correlation between any two antenna elements, and η_i is the total efficiency of the proposed MIMO antenna, which is depicted in Figure 12B. For the 2 elements MIMO antenna the acceptable range is 0.45 and in terms of dB, it is 3.5 dB. We can see that our proposed antenna is having a MUX efficiency of almost higher than 3.5 dB throughout the operating frequency.

4.5 | Channel capacity

The channel capacity is calculated by Equation (12),[39,45] which is directly proportional to the number of antenna elements. The results are shown in Figure 13. It gives information that how much bit rates you can achieve through the proposed MIMO antenna. Minimum and maximum channel capacity is 7.37 and 11.34 bps/Hz, respectively, at 20 dB signal-to-noise ratio (SNR) in a uniform environment.

$$C = k \log_2 \det\left(I + \frac{SNR}{k} HH^*\right) \quad (12)$$

In Equation (12), k denotes the number of antenna elements, I is the identity matrix and H denotes the fading matrix. While the upper level of the channel capacity of two antenna systems can be found out after considering there is no correlation among antenna elements and hence considering fading matrix [H] as identity matrix and then the channel capacity calculated from Equation (12) will be $C = 2 \log_2(1 + 100/2) = 11.344$ bps/Hz considering SNR = 20 dB = 100. The permissible value for two elements will be 65% of its maximum value[45] (11.344 bps/Hz) = 0.65 11.344 = 7.38 bps/Hz.

We can see that our calculated channel capacity of the proposed antenna is well above 10 bps/Hz throughout the operating frequency and below the maximum

TABLE 5 Comparison of the designed SWB-MIMO antenna with existing references in various aspects

Size (mm mm), $\lambda_0 \lambda_0 ¼ \lambda_0^2$	Frequency (GHz)	Efficiency/ 100	Peak Gain (dBi)	Max. ECC	CCL (bits/ s/Hz)	CP Band	No. of Antenna Elements	Min. DG (dB)	Isolation (dB)/ References
24 30, 0.24 0.30 = 0.07	3–12.6	0.7–0.8	4.8	0.05	0.2	0	2	9.85	17/6
17 33, 0.25 0.48 = 0.12	4.4–51.5	—	—	0.01	0.4	0	2	—	15/30
40 47, 0.17 0.20 = 0.03	1.3–40	0.8	6.7	0.02	—	0	2	9.99	20/31
63 63, 0.27 0.27 = 0.07	1.3–40	—	5.5	0.01	—	0	4	—	16/32
55.6 50.5, 0.29 0.27 = 0.08	1.575–40	0.5–0.9	4.78	0.005	0.35	2	2	9.98	20/39
19 30, 0.20 0.31 = 0.06	3.1–10.6	0.7–0.9	2.91	0.13	0.4	0	2	9.70	18/44
45 45, 0.33 0.33 = 0.11	2.2–13.5	0.7–0.9	6.8	0.04	—	1	4	9.9	18/46
70 68, 0.93 0.91 = 0.85	4–13	—	6.4	0.25	—	1	4	—	18/47
18 36, 0.18 0.36 = 0.06	3–40	—	4	0.01	—	0	2	9.98	55/33
50 30, 0.51 0.31 = 0.16	3.08–16	0.6–0.8	6	0.01	0.4	0	2	—	16/48
54 54, 0.55 0.55 = 030	3.1–12	0.80	7.5	0.015	<0.5	0	8	9.9	20/49
33.5 33.5, 0.13 0.13 = 0.017	1.15–40	—	5	0.005	—	0	4	—	18/50
36 24, 0.18 0.14 = 0.025	1.6–24.5	0.81	7.6	0.062	0.35	0	2	9.9	25/51
34 60, 0.26 0.46 = 0.12	2.3–18	—	6.3	0.004	—	0	2	9.9	20/52
49 54.5, 0.42 0.47 = 0.20	2.6–22	0.45–0.80	4.5	0.08	0.35	4	2	9.9	20/(Prop.)

channel capacity satisfying the eligibility criteria. The channel capacity will increase as you increase the number of elements.

4.6 | Mean effective gain (MEG)

Another important diversity parameter is the mean effective gain (MEG). MEG is the ratio of the mean received power by the ith antenna to the mean incident power of the jth antenna with the same route, $MEG_i = \varepsilon_{Total}/2$, where ε_{Total} is implying total effective efficiency of the ith antenna, that is, $\varepsilon^i_{Total} = \varepsilon^i_{mis}\,\varepsilon^{i,i}_{rad}$, and where $\varepsilon^i_{mis} = 1 - \sum_{j=1}^{N} |S_{ij}|^2$, $\varepsilon^i_{rad} = 1 - \sum_{j=1}^{N} |S_{ij}|^2$, where ε^i_{mis}, and ε^i_{rad} are mismatch efficiency and radiation efficiency of the ith antenna. The MEG ratio for the proposed MIMO antenna is examined by Equation (13).[39,43]

$$MEG = \frac{P_{rec}}{P_{inc}} = \int \frac{XPR\,G_{\theta i}(\Omega)P + G_{\phi i}(\Omega)P\,P_{\phi}(\Omega)P}{1 + XPR}\,d\Omega \quad (13)$$

where XPR is the cross-polarization ratio and $G_{\theta i}(\Omega)$, $G_{\phi i}(\Omega)$, and $P_{\phi}(\Omega)$ are the gain and power density functions of the incident wave, respectively, Ω is beam area. The computed MEG for XPR = 1 dB (outdoor) and 6 dB (indoor) in different mediums has been tabulated in Table 4 and also represented in Figure 14. We can observe that the radiated power is always less than stimulated and accepted power because of various losses like a surface wave, conductor, and dielectric losses. Power going to all ports is highly interfering with out-of-band frequencies than the intended band. Most of the power is correlated means coupled at port-1 to port-2 and not goes to radiation. In Table 4, we can find that the MEG is below the permissible value of ±3 dB for both indoor and outdoor irrespective of the assumed medium either Laplacian or Gaussian.

We have compared our proposed design with some existing UWB/SWB-MIMO antennas as tabulated in Table 5. The comparison is mainly focused on the number of CP bands and isolation achieved. We can observe that our proposed SWB-MIMO is having the maximum CP bands, that is, 4. Also, the isolation is comparable to all the tabulated MIMO antennas except.[33] We have a slightly bigger size antenna, 0.20 λ_0^2 in terms of free-space wavelength but we have an added advantage of a novel design having higher CP bands, comparable isolation, and low ECC computed through 3D-radiation patterns and easily fabricated on a readily available commercially cheap substrate FR-4. Also, the dimension is reasonable considering the UWB/SWB-MIMO antenna having a CP band and it has a lesser dimension than one structure[47] among these. The novelty of the designed antenna is 4 CP bands with an effective SAR value (1.095 W/kg at 3.5 GHz) due to the presence of EBG cells along with high isolation achieved due to a big U-shape slot introduced in the ground and the protruding F-shaped ground stub embedded with circular rings.

5 | CONCLUSIONS

In this article, a novel quad-band circularly polarized MIMO antenna has been proposed for SWB (2.6–22 GHz) wireless applications with minimum isolation of 17 dB (20 dB for the significant part) among antenna elements. All simulated results of the antenna have been verified with measured results over the entire impedance bandwidth. The antenna has achieved four circularly polarized bands: 5.2, 11.5, 14.66, and 16.75 GHz with 4.58 dBi peak gain, including omnidirectional radiation patterns with acceptable diversity performance like ECC, TARC, CCL, DG are 0.05, 10 dB, 0.35 bits/s/Hz and 9.9 dB, respectively. The average channel capacity is above 10.5 bps/Hz. The calculated SAR with the head voxel model is 1.095 W/kg at is 10 g of human body tissue. The performance of the proposed antenna is satisfactory in all respect, which means it is a good candidate for various portable wireless applications.

ACKNOWLEDGMENT

The authors acknowledge the CRS project having Application ID: 1-5748389248 sanctioned under TEQIP-III by the National Project Implementation Unit (NPIU), a unit of the Ministry of Human Resource Development (MHRD), Government of India.

DATA AVAILABILITY STATEMENT

Data sharing is not applicable to this article as no new data were created or analyzed in this study.

ORCID

Amit Kumar https://orcid.org/0000-0002-1871-8315
Gaurav Saxena https://orcid.org/0000-0002-3742-4961
Preetam Kumar https://orcid.org/0000-0003-3018-881X
Yogendra Kumar Awasthi https://orcid.org/0000-0001-8860-2329
Sumer Singh Singhwal https://orcid.org/0000-0002-8065-3284
Prashant Ranjan https://orcid.org/0000-0003-3377-7054

REFERENCES

1. Kumar A, Ansari AQ, Kanaujia BK, Kishor J, Matekovits L. A review on different techniques of mutual coupling reduction between elements of any MIMO antenna. Part 2: metamaterials and many more. Radio Sci. 2021;56(3). doi:10.1029/2020RS007222
2. Kumar A, Ansari AQ, Kanaujia BK, Kishor J, Matekovits L. A review on different techniques of mutual coupling reduction between elements of any MIMO antenna. Part 1: DGSs and parasitic structures. Radio Sci. 2021;56(3):1-25. doi:10.1029/2020RS007122
3. Luo XS, Bin Weng Z, Zhang WJ, Yang L. Compact planar multiband MIMO antenna based on composite right/left-handed transmission line for mobile phone applications. Microw Opt Technol Lett. 2018;60(6):1505-1511. doi:10.1002/mop.31185
4. Feng B, Lai J, Zeng Q, Chung KL. A dual-wideband and high gain magneto-electric dipole antenna and its 3D MIMO system with metasurface for 5G/WiMAX/WLAN/X-band applications. IEEE Access. 2018;6:33387-33398. doi:10.1109/ACCESS.2018.2848476
5. Chouhan S, Panda DK, Gupta M, Singhal S. Meander line MIMO antenna for 5.8 GHz WLAN application. Int J RF Microw Comput Eng. 2018;28(4):e21222. doi:10.1002/mmce.21222
6. Gurjar R, Upadhyay DK, Kanaujia BK, Kumar A. A compact modified sierpinski carpet fractal UWB MIMO antenna with square-shaped funnel-like ground stub. AEU – Int J Electron Commun. 2020;117:153126. doi:10.1016/j.aeue.2020.153126.
7. Banerjee J, Karmakar A, Ghatak R, Poddar DR. Compact CPW-fed UWB MIMO antenna with a novel modified Minkowski fractal defected ground structure (DGS) for high isolation and triple band-notch characteristic. J Electromagn Waves Appl. 2017;31(15):1550-1565. doi:10.1080/09205071.2017.1354727
8. Debnath P, Karmakar A, Saha A, Huda S. UMB MIMO slot antenna with minkowski fractal shaped isolators for isolation enhancement. Prog Electromagn Res M. 2018;75(October):69-78. doi:10.2528/PIERM18090506
9. Gurjar R, Upadhyay DK, Kanaujia BK, Kumar A. A compact u-shaped uwb-mimo antenna with novel complementary modified minkowski fractal for isolation enhancement. Prog Electromagn Res C. 2021;107(September 2020):81-96. doi:10.2528/pierc20091809
10. Rajkumar S, Vivek Sivaraman N, Murali S, Selvan KT. Heptaband swastik arm antenna for MIMO applications. IET Microw Antennas Propag. 2017;11(9):1255-1261. doi:10.1049/iet-map.2016.1098
11. Naser-Moghadasi M, Sadeghzadeh RA, Fakheri M, Aribi T, Sedghi T, Virdee BS. Miniature hook-shaped multiband antenna for mobile applications. IEEE Antennas Wirel Propag Lett. 2012;11:1096-1099. doi:10.1109/LAWP.2012.2214199
12. Lu D, Wang L, Yang E, Wang G. Design of high-isolation wideband dual-polarized compact MIMO antennas with multi-objective optimization. IEEE Trans Antennas Propag. 2018;66(3):1522-1527. doi:10.1109/TAP.2017.2784446
13. Chen SC, Wu PW, Hsu CIG, Sze JY. Integrated MIMO slot antenna on laptop computer for eight-band LTE/WWAN operation. IEEE Trans Antennas Propag. 2018;66(1):105-114. doi:10.1109/TAP.2017.2775284
14. Ghosh S, Tran TN, Le-Ngoc T. Dual-layer EBG-based miniaturized multi-element antenna for MIMO systems. IEEE Trans Antennas Propag. 2014;62(8):3985-3997. doi:10.1109/TAP.2014.2323410
15. Kumar A, Ansari AQ, Kanaujia BK, Kishor J. High isolation compact four-port MIMO antenna loaded with CSRR for multi-band applications. Frequenz. 2018;72(9–10):415-427. doi:10.1515/freq-2017-0276
16. Zhang YM, Zhang S, Li JL, Pedersen GF. A transmission-line-based decoupling method for MIMO antenna arrays. IEEE Trans Antennas Propag. 2019;67(5):3117-3131. doi:10.1109/TAP.2019.2900406
17. Ding C, Li Q, Yang Y, et al. A compact dual-band MIMO slot antenna for WLAN applications. 2018 IEEE Antennas Propag. Soc. Int. Symp. Usn. Natl. Radio Sci. Meet. APSURSI 2018 – Proc; 2018:461-462. doi:10.1109/APUSNCURSINRSM.2018.8608963
18. Liu L, Liu C, Li Z, Yin X, Chen ZN. Slit-slot line and its application to low cross-polarization slot antenna and mutual-coupling suppressed Tripolarized MIMO antenna. IEEE Trans Antennas Propag. 2019;67(1):4-15. doi:10.1109/TAP.2018.2876166
19. Ekrami H, Jam S. A compact triple-band dual-element MIMO antenna with high port-to-port isolation for wireless applications. AEU – Int J Electron Commun. 2018;96:219-227. doi:10.1016/j.aeue.2018.09.044
20. Li Y, Sim CYD, Luo Y, Yang G. Multiband 10-antenna Array for Sub-6 GHz MIMO applications in 5-G smartphones. IEEE Access. 2018;6:28041-28053. doi:10.1109/ACCESS.2018.2838337
21. DIcandia FA, Genovesi S, Monorchio A. Analysis of the performance enhancement of MIMO systems employing circular polarization. IEEE Trans Antennas Propag. 2017;65(9):4824-4835. doi:10.1109/TAP.2017.2723083
22. Huang FJ, Yo TC, Lee CM, Luo CH. Design of circular polarization antenna with harmonic suppression for rectenna application. IEEE Antennas Wirel Propag Lett. 2012;11:592-595. doi:10.1109/LAWP.2012.2201437
23. Pan Y, Cui Y, Qi CL, Li RL. Evaluation of dual-polarised triple-band multi-beam MIMO antennas for WLAN/WiMAX applications. IET Microw Antennas Propag. 2017;11(10):1469-1475. doi:10.1049/iet-map.2016.1101
24. Alsath MGN, Arun H, Selvam YP, et al. An integrated triband/UWB polarization diversity antenna for vehicular networks. IEEE Trans Veh Technol. 2018;67(7):5613-5620. doi:10.1109/TVT.2018.2806743
25. Islam SN, Kumar M, Sen G, Das S. Design of a compact triple band antenna with independent frequency tuning for MIMO applications. Int J RF Microw Comput Eng. 2019;29(3):e21620. doi:10.1002/mmce.21620
26. Hussain R, Sharawi MS, Shamim A. An integrated four-element slot-based MIMO and a UWB sensing antenna system for CR platforms. IEEE Trans Antennas Propag. 2018;66(2):978-983. doi:10.1109/TAP.2017.2781220
27. Srivastava K, Kumar S, Kanaujia BK, Dwari S. Design and packaging of ultra-wideband multiple-input-multiple-output/diversity antenna for wireless applications. Int J RF Microw Comput Eng. 2020;30(10):1-10. doi:10.1002/mmce.22357
28. Srivastava K, Kumar S, Kanaujia BK, Dwari S, Choi HC, Kim KW. Compact eight-port MIMO/diversity antenna with band rejection characteristics. Int J RF Microw Comput Eng. 2020;30(5):1-13. doi:10.1002/mmce.22170

29. Srivastava K, Kanaujia BK, Dwari S, Kumar S, Khan T. 3D cuboidal design MIMO/diversity antenna with band notched characteristics. AEU – Int J Electron Commun. 2019;108:141-147. doi:10.1016/j.aeue.2019.06.018
30. Singhal S. Feather-shaped super wideband MIMO antenna. Int J Microw Wirel Technol. 2021;13(1):94-102. doi:10.1017/S1759078720000549
31. Ullah H, Rahman SU, Cao Q, Khan I, Ullah H. Design of SWB MIMO antenna with extremely wideband isolation. Electronics. 2020;9(1):194. doi:10.3390/electronics9010194
32. Kumar P, Urooj S, Alrowais F. Design of quad-port MIMO/diversity antenna with triple-band elimination characteristics for super-wideband applications. Sensors. 2020;20(3):624. doi:10.3390/s20030624
33. Khan MI, Khattak MI, Ur Rahman S, Qazi AB, Telba AA, Sebak A. Design and investigation of modern UWB-MIMO antenna with optimized isolation. Micromachines. 2020;11(4):432. doi:10.3390/MI11040432
34. Abd-Alhameed RA, Mangoud M, Excell PS, Khalil K. Investigations of polarization purity and specific absorption rate for two dual-band antennas for satellite-mobile handsets. IEEE Trans Antennas Propag. 2005;53(6):2108-2110. doi:10.1109/TAP.2005.848516
35. Balanis CA. Antenna Theory: Analysis and Design. 4th ed. John wiley& sons; 2016.
36. Modak S, Khan T, Laskar RH. Penta-notched UWB monopole antenna using EBG structures and fork-shaped slots. Radio Sci. 2020;55(9):1-2. doi:10.1029/2019RS006983
37. Alam MS, Misran N, Yatim B, Islam MT. Development of electromagnetic band gap structures in the perspective of microstrip antenna design. Int J Antennas Propag. 2013;2013:507158. doi:10.1155/2013/507158
38. Kim S-H, Nguyen TT, Jang J-H. Reflection characteristics of 1-d EBG ground plane and its application to a planar dipole antenna. Prog Electromagn Res. 2011;120:51-66. doi:10.2528/PIER11062909
39. Saxena G, Jain P, Awasthi YK. High diversity gain super-wideband single band-notch MIMO antenna for multiple wireless applications. IET Microw Antennas Propag. 2020;14(1):109-119. doi:10.1049/iet-map.2019.0450
40. Iyama T, Onishi T, Tarusawa Y, Uebayashi S, Nojima T. Novel specific absorption rate (SAR) measurement method using a flat solid phantom. IEEE Trans Electromagn Compat. 2008;50(1):43-51. doi:10.1109/TEMC.2007.913216
41. Sharawi MS, Khan MU, Numan AB, Aloi DN. A CSRR loaded MIMO antenna system for ISM band operation. IEEE Trans Antennas Propag. 2013;61(8):4265-4274. doi:10.1109/TAP.2013.2263214
42. Kumar A, Ansari AQ, Kanaujia BK, Kishor J. Dual circular polarization with reduced mutual coupling among two orthogonally placed CPW-fed microstrip antennas for broadband applications. Wirel Pers Commun. 2019;107(2):759-770. doi:10.1007/s11277-019-06298-x
43. Saxena G, Jain P, Awasthi YK. High diversity gain MIMO-antenna for UWB application with WLAN notch band characteristic including human Interface devices. Wirel Pers Commun. 2020;112(1):105-121. doi:10.1007/s11277-019-07018-1
44. Kumar A, Ansari AQ, Kanaujia BK, Kishor J, Kumar S. An ultra-compact two-port UWB-MIMO antenna with dual band-notched characteristics. AEU – Int J Electron Commun. 2020;114:152997. doi:10.1016/j.aeue.2019.152997
45. Loyka SL. Channel capacity of MIMO architecture using the exponential correlation matrix. IEEE Commun Lett. 2001;5(9):369-371. doi:10.1109/4234.951380
46. Kumar P, Urooj S, Malibari A. Design of Quad-Port Ultra-Wideband Multiple-Input-Multiple-Output Antenna with wide axial-ratio bandwidth. Sensors. 2020;20(4):1174. doi:10.3390/s20041174
47. Kumar S, Lee GH, Kim DH, Choi HC, Kim KW. Dual circularly polarized planar four-port mimo antenna with wide axial-ratio bandwidth. Sensors. 2020;20(19):1-19. doi:10.3390/s20195610
48. Kumar A, Ansari AQ, Kanaujia BK, Kishor J, Tewari N. Design of Triple-Band MIMO antenna with one band-notched characteristic. Prog Electromagn Res C. 2018;86:41-53. doi:10.2528/PIERC18051902
49. Palanisamy P, Subramani M. Design and experimental analysis of miniaturized Octa-port UWB/SWB-MIMO antenna with triple-band rejection characteristics. IETE J Res. 2020:1-15. doi:10.1080/03772063.2020.1798824
50. Kumar Raheja D, Kumar S, Kumar Kanaujia B, Kumar Palaniswamy S, Rao Thipparaju R, Kanagasabai M. Truncated elliptical Self-Complementary antenna with Quad-Band notches for SWB MIMO systems. AEU – Int J Electron Commun. 2021;131(May 2020):153608. doi:10.1016/j.aeue.2021.153608
51. Singh AK, Mahto SK, Sinha R. Compact super-wideband MIMO antenna with improved isolation for wireless communications. Frequenz. 2021;75(9–10):407-417. doi:10.1515/freq-2020-0213
52. Bahmanzadeh F. SWB MIMO antenna with dual band rejection characteristics and polarization diversity for UWB applications. Res Square. 2021:1-22. doi:10.21203/rs.3.rs-555061/v1